International Journal of Advanced Geosciences, 14 (1) (2026) 79-87

International Journal of Advanced Geosciences

Website: www.sciencepubco.com/index.php/IJAG
https://doi.org/10.14419/84vmsj09
Research paper

Geochemical Constraints on Provenance, Paleoweathering, And Paleodepositional Conditions of The Mamu Formation Along Apana–Imiegba Road, Western Anambra Basin, Nigeria

Kehinde Omokinde[1], Solomon Olupona[1], Olutayo Ayeniyo [2,4]*, Oladotun Oluwajana[3], Temitayo Ale[1]

[1]*Department of Earth Sciences, Adekunle Ajasin University, Akungba-Akoko, Ondo State, Nigeria*
[2]*School of Earth, Environment, and Sustainability, University of Iowa, Iowa City, USA*
[3]*Department of Applied Geology, Olusegun Agagu University of Science and Technology, Okitipupa, Ondo State, Nigeria*
[4]*Columbine Corporation, Texas, USA*
**Corresponding author E-mail: olutayo-ayeniyo@uiowa.edu*

Received: 24-06-2026, Accepted: 24-06-2026, Published: 05-08-2026

Abstract

The Late Cretaceous Mamu Formation in the western Anambra Basin consists of transitional deltaic to shallow marine deposits that record changes in sediment source, weathering, salinity, redox conditions, and depositional processes. This study uses major and trace element geochemistry of outcrop samples collected along the Apana–Imiegba road to assess provenance, paleoweathering, and paleodepositional conditions. Major-element indices, including CIA, PIA, and CIW, indicate strong chemical weathering of the source area, consistent with warm and humid paleoclimatic conditions. Provenance-sensitive ratios such as Al_2O_3/TiO_2 and Fe_2O_3/TiO_2 suggest derivation mainly from felsic continental source rocks, with limited evidence of sediment recycling. Trace element ratios, including Sr/Ba and Sr/Cu, point to fluctuating brackish to marginal marine conditions, while redox-sensitive proxies such as V/Cr, U/Th, and Cu/Zn indicate suboxic to weakly anoxic bottom-water conditions, especially in shale-rich intervals. Relative enrichment in phosphorus and barium, together with higher P/Ti values in some intervals, may indicate episodic productivity under favorable preservation conditions. Overall, the Mamu Formation along the Apana–Imiegba road reflects deposition in a humid, delta-influenced basin marked by variable salinity, fluctuating redox conditions, and mixed continental to marginal marine influence.

Keywords: *Mamu Formation; Anambra Basin; Sediment Geochemistry; Provenance; Paleoweathering; Paleoenvironmental Reconstruction.*

1. Introduction

Sedimentary geochemistry is useful for understanding where sediments came from, how strongly they were weathered, and the conditions under which they were deposited. In siliciclastic basins, the chemical composition of sediments can record source-rock type, climate, transport history, redox conditions, and depositional processes [1], [2]. Major oxides and trace elements are commonly used for this type of interpretation. Relatively immobile oxides such as Al_2O_3 and TiO_2, together with indices such as CIA, PIA, and CIW, help assess source composition and chemical weathering intensity [3–5]. Trace elements such as V, Cr, U, Th, Sr, Ba, Cu, and Zn can also provide information on redox conditions, salinity, climate, and productivity when interpreted alongside field observations [6], [1], [7].

The Mamu Formation is a Late Cretaceous coal-bearing unit in the Anambra Basin. It consists mainly of sandstone, shale, carbonaceous mudstone, and coal seams, and is generally linked to transitional deltaic to shallow marine deposition [8], [9]. The Anambra Basin formed after the Santonian tectonic inversion, which shifted sedimentation from the Abakaliki Trough into the Anambra platform [10], [11]. Its major stratigraphic units include the Nkporo, Mamu, Ajali, and Nsukka Formations, deposited in environments ranging from shallow marine to fluvial settings [12], [13].

Although the Mamu Formation has been studied for its stratigraphy, sedimentology, palynology, and coal deposits, fewer studies have used both major and trace element geochemistry to interpret the western margin of the basin, especially around the Apana–Imiegba area [14], [15]. Because of this, the links between provenance, weathering, salinity, redox conditions, and depositional setting in this area are still not well defined.

This study uses major and trace element data from Mamu Formation outcrops along the Apana–Imiegba road, western Anambra Basin (Fig. 1). The objectives are to: (1) determine sediment provenance and weathering intensity, (2) reconstruct paleoredox, paleosalinity, and paleoclimatic conditions, and (3) interpret the depositional environment using geochemical proxies supported by field observations.

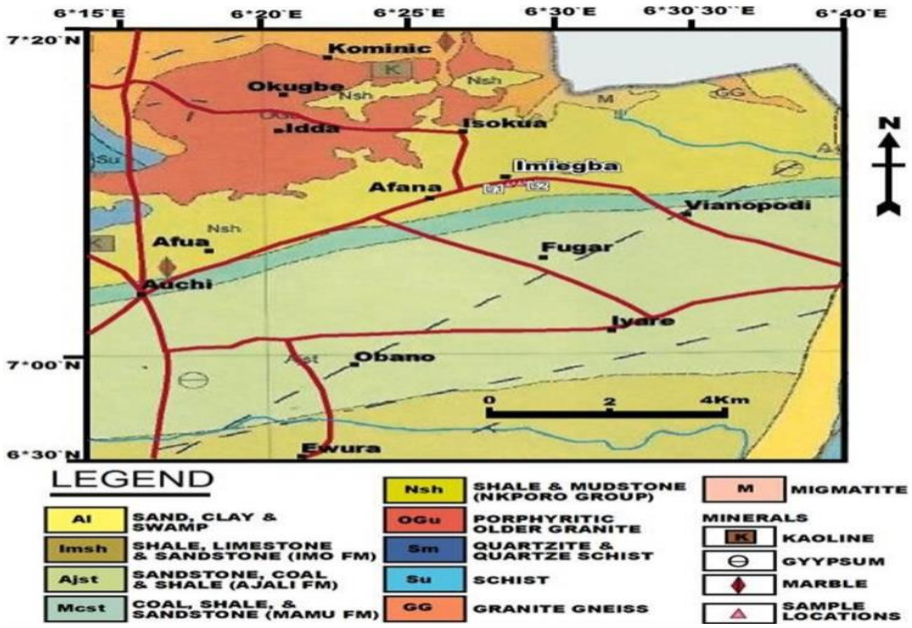

Fig. 1: Location Map of the Study Area Adapted from Jayeola Et Al. (2016).

1.1. Stratigraphic setting of the Anambra Basin

The Anambra Basin succession includes the Nkporo Group, Mamu Formation, Ajali Formation, Nsukka Formation, and Imo Formation. The Mamu Formation, which is the focus of this study, is a Maastrichtian coal-bearing unit made up of alternating shale, siltstone, fine-grained sandstone, sandy shale, ironstone, and thin coal seams. It is generally interpreted as a deltaic to marginal marine deposit formed during repeated marine transgressions and regressions [17-19]. The overlying Ajali Formation records a shift toward higher-energy sandy deposition, while the Nsukka Formation represents a later transgressive phase with tidal flat, lagoonal, bay, and shoreface deposits [20, 21]. This stratigraphic context is important because the Mamu Formation records the transitional conditions targeted in this study. The regional geological setting and stratigraphic succession are shown in Figs. 2 and 3.

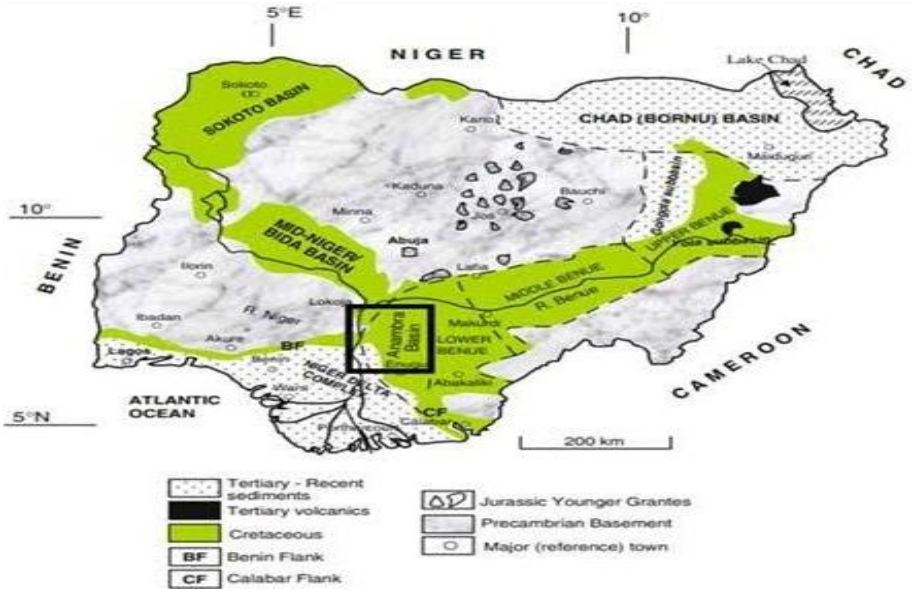

Fig. 2: Geological Map of Nigeria Showing the Anambra Basin within the Rectangular Outline Modified After Obaje [22].

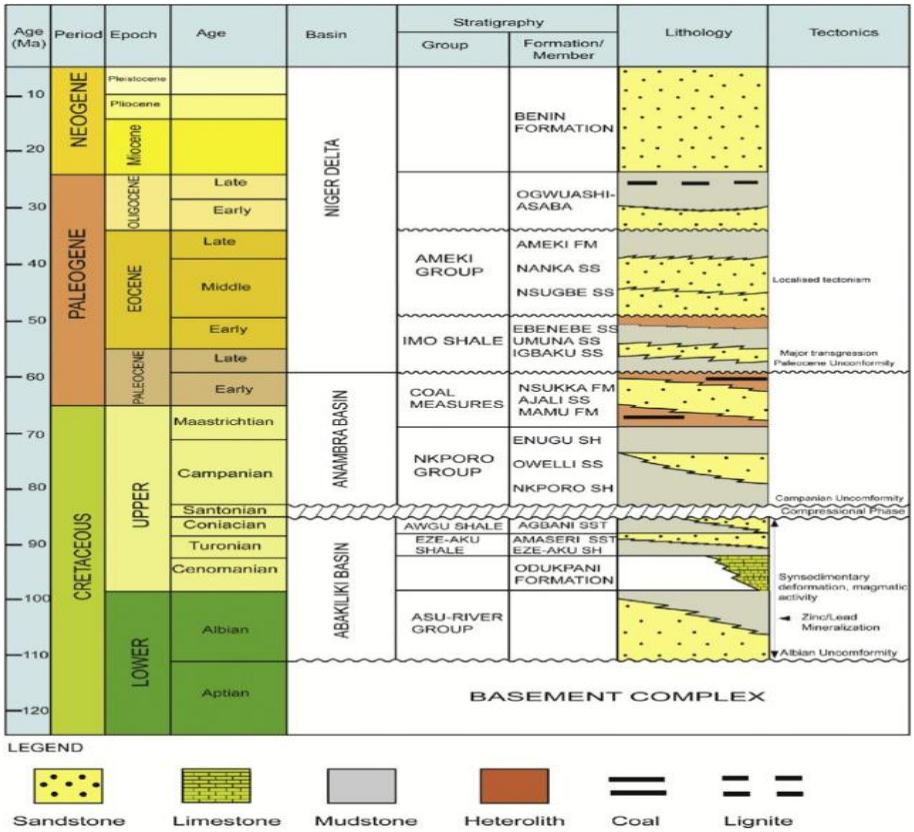

Fig. 3: Stratigraphic Succession of the Anambra Basin and Niger Delta Redrawn and Modified from Nwajide [23].

2. Materials and Methods

Shale and sandstone samples were collected from a well-exposed section of the Mamu Formation along the Apana–Imiegba road in Etsako East Local Government Area, Edo State, on the western flank of the Anambra Basin (Fig. 2). The studied exposure is approximately 44.59 m thick and consists of alternating grey shale, fine-grained sandstone, ironstone lenses, and minor coal seams. A total of fourteen fresh samples were collected from representative lithologic units across the section. Field logging was carried out using a geological hammer, compass-clinometer, GPS, and hand lens. Bedding characteristics, lithology, grain size, sedimentary structures, colour, and textural variations were recorded systematically. Each sample was labeled, sealed in clean sample bags, and transported to the laboratory for geochemical analysis.

In the laboratory, the samples were air-dried and pulverized to less than 75 μm using a tungsten carbide ring mill. The pulverized samples were then split into aliquots for major and trace element analyses. Major oxides were determined by X-ray fluorescence (XRF) using an ARL9400XP+ wavelength-dispersive spectrometer equipped with a Rh tube and standard analyzing crystals (LiF220, AXO6, GER, PET), following Loubser and Verryn [24]. Trace elements were analyzed using inductively coupled plasma mass spectrometry (ICP-MS) on a Thermo Scientific iCAP RQ system at the Earth Laboratory, University of the Witwatersrand, Johannesburg. The major oxides analyzed include SiO_2, Al_2O_3, Fe_2O_3, MgO, CaO, Na_2O, K_2O, TiO_2, and MnO. These data were used to calculate weathering indices, including the Chemical Index of Alteration (CIA), Plagioclase Index of Alteration (PIA), and Chemical Index of Weathering (CIW). All oxide values were converted to molar proportions before calculation. CIA was calculated as:

$$\mathrm{CIA} = \left\{ {}^{\mathrm{Al_2O_3}} \Big/ {}_{(\mathrm{Al_2O_3} + \mathrm{CaO^*} + \mathrm{Na_2O} + \mathrm{K_2O})} \right\} \times 100$$

Where CaO* represents CaO associated with the silicate fraction. For CaO* correction, CaO* was taken as the lower value of CaO and Na_2O after conversion to molar proportions. PIA and CIW values were calculated following Fedo et al. [5] and Harnois [4], respectively.

The trace elements analyzed include Rb, Sr, Ba, P, Ti, V, Cr, U, Th, Ni, Cu, and Zn. Selected trace element ratios were used to infer paleoenvironmental conditions. V/Cr, U/Th, and Cu/Zn were used to assess paleoredox conditions, while Sr/Ba and Sr/Cu were used to evaluate paleosalinity and paleoclimate. P/Ti was used cautiously as a relative indicator of productivity. Provenance was assessed using Al_2O_3/TiO_2, Fe_2O_3/TiO_2, and Al_2O_3–Fe_2O_3–MnO discrimination plots. Sediment recycling was interpreted cautiously, based on geochemical trends and field evidence rather than a single proxy.

3. Results

3.1. Lithological description and field observations

The logged outcrop of the Mamu Formation along the Apana–Imiegba road shows alternating shale, sandstone, ironstone, and minor coal-bearing intervals. Representative field features are shown in Figs. 4 and 5, while the logged lithologic section is presented in Fig. 6. The basal part of the section is dominated by massive dark-grey shale. The shale is moderately fissile and locally ferruginized, with minor silt-rich lamination. Some horizons show fine lamination, iron staining, and small root traces. Above the basal shale, fine- to medium-grained

sandstone beds occur. These sandstones are grey to light brown, moderately sorted, and quartz-rich. Ripple lamination, soft-sediment deformation, occasional cross-bedding, and sharp erosive basal contacts are also present.

A thin, laterally discontinuous coal layer, about 0.3–0.5 m thick, occurs near the middle of the section. It is associated with carbonaceous shale. Ironstone beds occur as nodular to laminated horizons within the shale-rich intervals. Toward the upper part of the section, sandstone beds become thicker, reaching about 1.5 m, and are commonly planar laminated to structureless, with occasional bioturbation.

Fig. 4: Field Photograph Showing Wavy Lamination within Sandstone–Shale Interbeds of the Mamu Formation

Fig. 5: Field Photograph Showing Fractured Shale and Ferruginized Horizons within the Mamu Formation Outcrop.

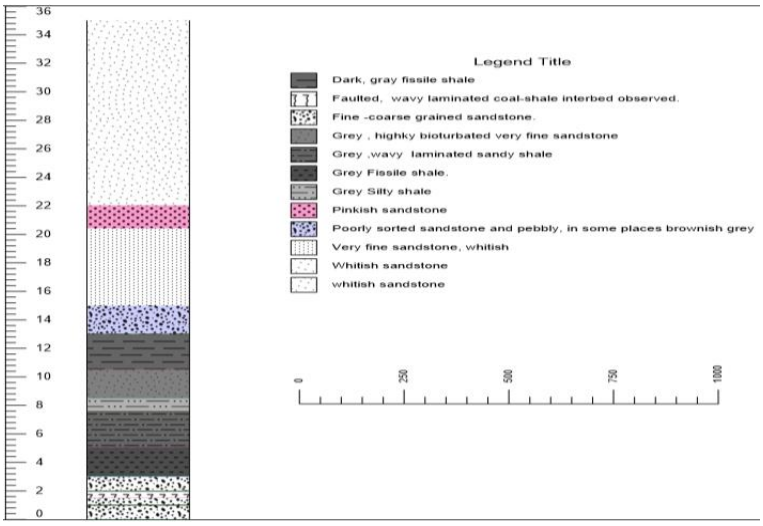

Fig. 6: Lithologic Section of the Mamu Formation Exposed at Apana–Imiegba.

3.2. Major oxide geochemistry

The major oxide composition of the samples is dominated by SiO_2 and Al_2O_3, with lower amounts of Fe_2O_3, TiO_2, MgO, K_2O, Na_2O, and MnO (Table 1). SiO_2 ranges from 52.31 to 68.14 wt.%, while Al_2O_3 ranges from 12.90 to 20.56 wt.%. Fe_2O_3 is higher in some shale samples, which matches the field evidence of ferruginization and ironstone layers. The Al_2O_3/TiO_2 ratio ranges from 16.52 to 20.41. K_2O/Na_2O ratios are relatively high in most samples. TiO_2 values are mostly below 1.5 wt.%, while MgO and CaO occur in low amounts. The Al_2O_3–Fe_2O_3–MnO ternary plot is shown in Fig. 7. The calculated weathering indices are presented in Table 2.

Table 1: Major Oxide Composition of Shale And Sandstone Samples from the Mamu Formation Exposed Along the Apana–Imiegba Road

Sample	SiO_2	Al_2O_3	Fe_2O_3	MnO	MgO	CaO	Na_2O	K_2O	TiO_2	P_2O_5	Cr_2O_3	NiO	LOI	Total
SH01	53.70	26.54	3.21	0.01	0.42	0.06	0.02	1.31	1.64	0.14	0.02	0.00	13.10	100.16
SH03	71.55	12.51	1.42	0.01	0.11	0.07	0.01	0.49	1.18	0.06	0.01	0.00	11.87	99.30
SH04	49.87	27.33	3.82	0.01	0.46	0.12	0.01	1.37	1.26	0.31	0.03	0.00	15.50	100.10
SH06	56.33	24.19	3.09	0.01	0.48	0.10	0.02	1.57	0.97	0.28	0.02	0.00	13.02	100.09
SH07	49.36	32.13	3.12	0.01	0.38	0.06	0.02	1.21	1.25	0.13	0.02	0.00	12.80	100.50
ST01	79.11	11.69	0.88	0.00	0.06	0.05	0.00	0.10	1.28	0.08	0.01	0.00	4.89	98.15
ST02	75.35	15.70	0.79	0.01	0.06	0.05	0.00	0.10	1.01	0.09	0.01	0.00	5.88	99.03

Table 2: Major Oxide Weathering Indices of Shale and Sandstone Samples from the Apana–Imiegba Section

Sample	CIA	PIA	CIW
SH01	94.71	99.74	99.75
SH03	95.69	99.73	99.74
SH04	94.75	99.87	99.88
SH06	93.20	99.71	99.73
SH07	95.89	99.79	99.80
ST01	99.08	100.00	100.00
ST02	99.32	100.00	100.00

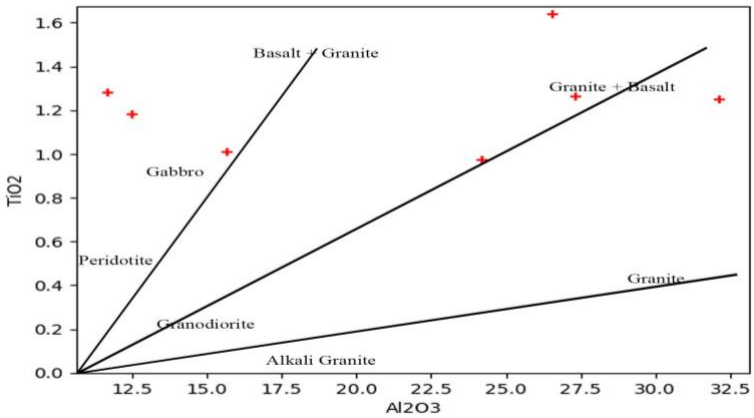

Fig. 7: Al_2O_3 Versus Tio_2 Cross Plot Showing Source-Rock Composition.

3.3. Weathering intensity and chemical maturity

CIA values range from 93.20 to 99.32, indicating very intense chemical weathering of the source materials. PIA values range from 99.71 to 100.00, suggesting near-complete alteration of plagioclase feldspar. CIW values range from 99.73 to 100.00, further supporting extreme chemical alteration under humid climatic conditions. Chemical maturity is further shown by the SiO_2 versus $Al_2O_3 + K_2O + Na_2O$ plot (Fig. 8). Provenance and weathering trends are also shown by the Al_2O_3–Fe_2O_3–MnO and Al_2O_3–CaO + Na_2O–MnO ternary plots (Figs. 9 and 10).

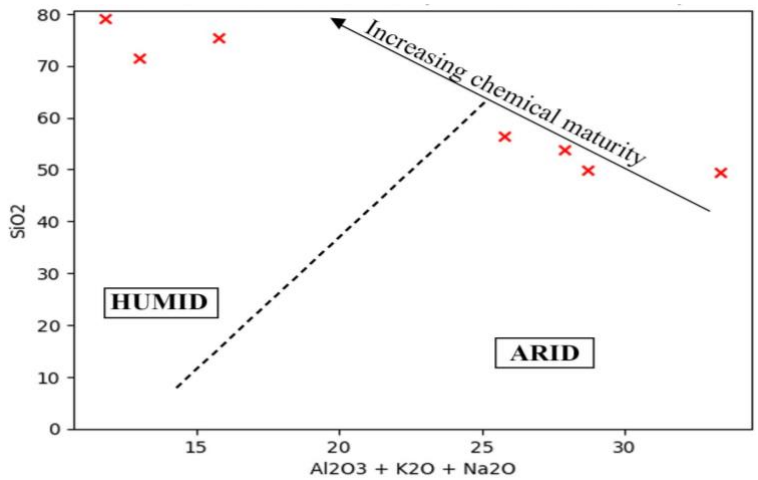

Fig. 8: Sio_2 Versus $Al_2O_3 + K_2O + Na_2O$ Plot Showing Chemical Maturity.

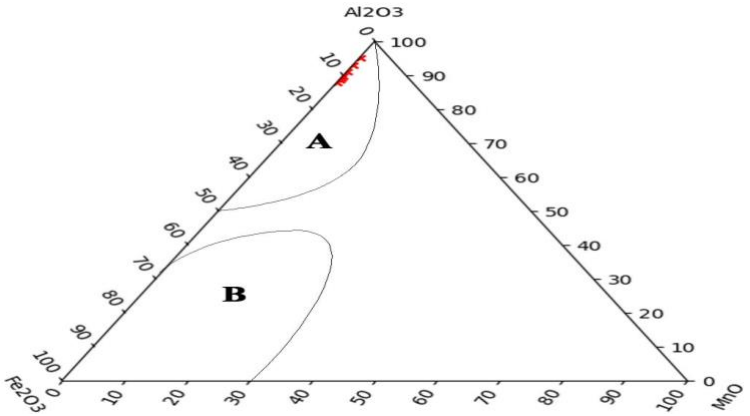

Fig. 9: Al_2O_3–Fe_2O_3–Mno Ternary Plot Showing Provenance Variation.

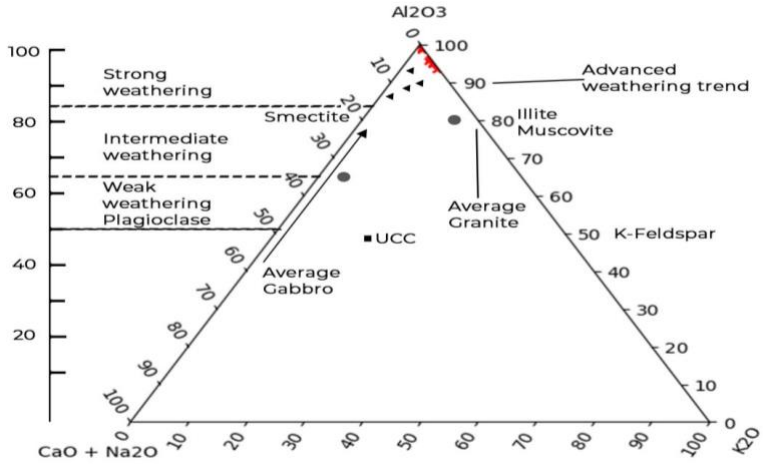

Fig. 10: Al_2O_3–Cao + Na_2O–Mno Ternary Plot Showing Chemical Weathering Trend.

3.4. Trace element geochemistry

Trace element concentrations are presented in Table 3, while calculated trace element ratios are shown in Table 4. V/Cr values range from 1.17 to 2.53. U/Th values range from 0.59 to 1.04, while Cu/Zn values range from 0.36 to 0.66.

Table 3: Trace Element Concentrations of Shale and Sandstone Samples from the Mamu Formation Exposed Along the Apana–Imiegba Road

Sample	Rb	Sr	Ba	P	Ti	V	Cr	U	Th	Ni	Cu	Zn
SH-01	74.159	74.672	173.653	458.680	10902.765	154.455	124.216	7.832	25.634	25.253	17.89	48.009
SH-03	22.054	41.066	99.284	159.142	7073.568	47.736	60.248	12.791	19.559	9.818	11.46	24.640
SH-04	60.706	71.332	158.149	842.231	7394.149	160.244	122.537	8.431	26.336	30.226	8.88	50.629
SH-06	75.353	66.135	132.589	713.659	5692.353	111.230	116.955	4.937	23.815	40.891	4.20	31.386
SH-07	44.165	58.201	140.472	292.235	7058.297	115.553	122.610	5.599	11.212	21.311	11.67	29.218
ST-01	6.1980	59.874	66.5860	209.422	7655.700	47.109	65.361	4.276	24.437	8.543	1.94	14.677
ST-02	4.3870	116.922	138.831	300.115	6588.579	45.189	55.589	3.381	19.932	10.857	1.69	22.155

Table 4: Calculated Trace Element Ratios Used for Paleoredox, Paleosalinity, Paleoclimate, And Paleoproductivity Interpretation

Sample	Rb/Sr	Sr/Ba	P/Ti	V/Cr	U/Th	Sr/Cu
SH-01	0.99	0.43	0.04	1.24	0.31	4.17
SH-03	0.54	0.41	0.02	0.79	0.65	3.58
SH-04	0.85	0.45	0.11	1.31	0.32	8.03
SH-06	1.14	0.50	0.13	0.95	0.21	15.75
SH-07	0.76	0.41	0.04	0.94	0.50	4.69
ST-01	0.10	0.90	0.03	0.72	0.17	30.86
ST-02	0.04	0.84	0.05	0.81	0.17	69.18

3.5. Paleosalinity and paleoclimate proxies

Sr/Ba values in shale samples range from 0.41 to 0.50. In contrast, very fine-grained sandstone samples show higher Sr/Ba values of 0.84 to 0.90. Sr/Cu values show wide variation, ranging from 3.58 to 69.18, with markedly higher values in some sandstone samples. The Sr/Cu versus Rb/Sr cross plot is shown in Fig. 11. Some shale intervals also show Ba enrichment, while Cu and Zn show moderate enrichment in selected samples.

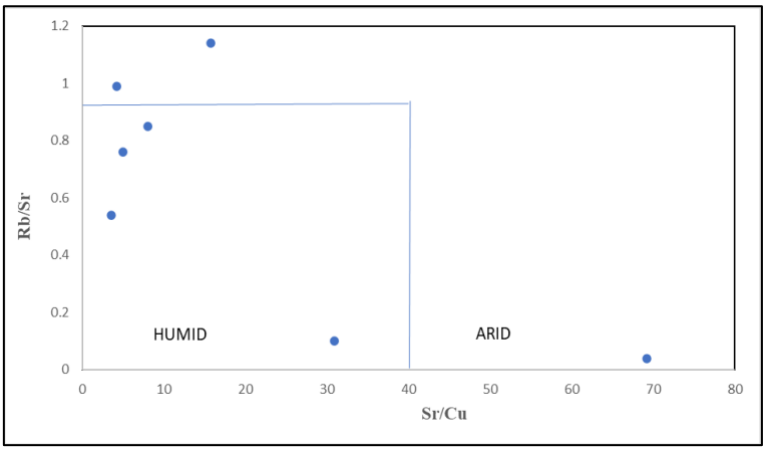

Fig. 11: Sr/Cu Versus Rb/Sr Cross Plot Showing Paleoclimatic Conditions.

4. Discussion

4.1. Provenance and source-area characteristics

The dominance of SiO_2 and Al_2O_3 suggests that the sediments are mainly quartz- and clay-rich. The Al_2O_3/TiO_2 values, which range from 16.52 to 20.41, point to a mainly felsic to intermediate source based on the classification of Hayashi et al. [25]. The relatively high K_2O/Na_2O ratios also support input from weathered continental crust.

The Al_2O_3–Fe_2O_3–MnO ternary plot supports this interpretation, with most samples plotting close to the Al_2O_3 corner. This suggests a strong clay-rich or weathered continental source. The source materials may have been supplied from nearby basement terrains such as the Oban Massif and Cameroon Basement Complex, which contain granitic and gneissic rocks [10].

Low TiO_2 values, together with low MgO and CaO, suggest limited mafic and carbonate input. However, sediment recycling cannot be strongly confirmed from these proxies alone. Stronger evidence would require ratios such as Zr/Sc or Th/Sc.

4.2. Paleoweathering and paleoclimate

The CIA, PIA, and CIW results show strong chemical weathering of the source materials. CIA values above 80 are commonly linked to intense leaching of mobile elements such as Ca, Na, and K under humid conditions (Nesbitt and Young, 1982). The high PIA values also show strong alteration of plagioclase feldspar, which supports advanced feldspar breakdown during chemical weathering [5].

CIW values further support intense chemical alteration. Since CIW excludes K_2O, it reduces the possible effect of K-metasomatism during diagenesis [4]. Overall, these indices point to strong chemical weathering under a warm and humid paleoclimate, consistent with wider reconstructions of tropical conditions in West Africa during the Late Cretaceous [26].

The high CIA, PIA, and CIW values support strong chemical weathering of the source materials.

4.3. Redox conditions and organic matter preservation

The redox ratios suggest that oxygen levels changed during deposition. V/Cr values between 1.0 and 2.0 generally suggest dysoxic to suboxic conditions, while values above 2 may indicate more reducing conditions [27]. Since the V/Cr values in this study range from 1.17 to 2.53, the sediments were likely deposited under dysoxic to suboxic conditions, with weakly anoxic episodes in some intervals.

U/Th values also support variable oxygen conditions. Uranium is usually enriched under reducing conditions, while thorium is relatively immobile. Higher U/Th values therefore suggest lower oxygen conditions [28]. The U/Th values in this study suggest changes from more oxygenated intervals to more reducing shale-rich intervals. Cu/Zn values range from 0.36 to 0.66, suggesting fluctuating oxic to suboxic conditions rather than continuous anoxia. When V/Cr, U/Th, and Cu/Zn are considered together, they show that oxygen conditions were variable during deposition. More reducing conditions likely occurred in organic-rich shale and coal-bearing intervals, while sandstone-rich layers reflect better circulation and higher energy.

This interpretation agrees with field evidence such as laminated shale, coal streaks, ferruginized beds, and ironstone layers. These features suggest repeated changes between restricted, quiet-water conditions and more oxygenated phases.

4.4. Paleosalinity, paleoclimate, and hydrodynamic conditions

Sr/Ba values suggest changes in salinity during deposition [29], [2]. The shale samples have Sr/Ba values of 0.41 to 0.50, which suggest brackish-water conditions. The very fine-grained sandstone samples have higher Sr/Ba values of 0.84 to 0.90, suggesting stronger marine influence. Together, these values point to a marginal marine to brackish setting affected by freshwater input and occasional marine incursions.

Sr/Cu values show considerable variability, with some shale samples falling within the humid climatic range, while higher values in sandstone samples may reflect low Cu concentrations, sediment compositional effects, or post-depositional modification rather than a purely arid climatic signal.

4.5. Paleoproductivity and depositional environment

Paleoproductivity was interpreted using phosphorus, P/Ti ratios, and selected trace elements. P/Ti values show relative increases in some shale-rich intervals. These increases may reflect short periods of higher productivity, better phosphorus preservation, or restricted bottom-

water conditions. However, phosphorus can also be affected by detrital input, redox cycling, and diagenesis, so P/Ti is best interpreted together with field and redox evidence [1], [29].
Some shale intervals also show Ba enrichment, which may suggest periods of increased biogenic input [30], [1]. However, Ba can also be affected by detrital and diagenetic processes. Moderate Cu and Zn enrichment in some samples supports periods of organic matter accumulation under lower oxygen conditions. When combined with coal streaks, laminated shale, ferruginized beds, and the redox ratios, the data suggests that organic matter was better preserved during restricted, low-energy phases.
Taken together, the field and geochemical evidence indicate that the Mamu Formation at Apana–Imiegba was deposited in a transitional deltaic to marginal marine setting. The shale and coal-bearing intervals reflect quiet-water, organic-rich, and locally restricted conditions. The sandstone beds record higher-energy phases, likely related to distributary channel, mouth-bar, or crevasse-splay activity. This interpretation agrees with earlier descriptions of the Mamu Formation as a coal-bearing unit deposited in delta-plain to marginal marine settings [8], [31].

5. Conclusion

This study shows that the Mamu Formation exposed along the Apana–Imiegba road was mainly derived from felsic to intermediate continental source rocks that experienced intense chemical weathering under warm and humid climatic conditions. The very high CIA, PIA, and CIW values indicate strong leaching of mobile elements and advanced alteration of feldspar-rich source materials.
Trace element ratios suggest deposition under fluctuating brackish to marginal marine conditions, with variable oxygen levels ranging from dysoxic to suboxic and occasional weakly anoxic episodes in shale-rich intervals. Sr/Ba values indicate mixed freshwater and marine influence, while V/Cr, U/Th, and Cu/Zn ratios point to restricted bottom-water conditions that favored organic matter preservation. Relative enrichment in phosphorus and barium also suggests episodic productivity during deposition.
Overall, the field and geochemical evidence indicate that the Apana–Imiegba section of the Mamu Formation was deposited in a transitional deltaic to marginal marine setting influenced by humid climate, continental sediment supply, marine incursions, and fluctuating redox conditions. Further studies using rare earth elements, mineralogical data, and additional provenance-sensitive ratios such as Zr/Sc and Th/Sc are recommended to better constrain sediment recycling, source-rock composition, and basin evolution.

Acknowledgements

Not applicable

Funding

No funding was received for conducting this study.

Competing interests

The authors have no competing interests to declare that are relevant to the content of this article.

References

[1] Tribovillard, N., Algeo, T. J., Lyons, T. W., & Riboulleau, A. (2006). Trace metals as paleoredox and paleoproductivity proxies: An update. Chemical Geology, 232, 12–32. https://doi.org/10.1016/j.chemgeo.2006.02.012.
[2] Zhang, K., Liu, R., Liu, Z., Li, L., Wu, X., & Zhao, K. (2020). Influence of palaeoclimate and hydrothermal activity on organic matter accumulation in lacustrine black shales of the Lower Cretaceous Bayingebi Formation, Yin'e Basin, China. Palaeogeography, Palaeoclimatology, Palaeoecology, 560, 110007. https://doi.org/10.1016/j.palaeo.2020.110007.
[3] Nesbitt, H. W., & Young, G. M. (1982). Early Proterozoic climates and plate motions inferred from major element chemistry of lutites. Nature, 299, 715–717. https://doi.org/10.1038/299715a0.
[4] Harnois, L. (1988). The CIW index: A new chemical index of weathering. Sedimentary Geology, 55, 319–322. https://doi.org/10.1016/0037-0738(88)90137-6.
[5] Fedo, C. M., Nesbitt, H. W., & Young, G. M. (1995). Unravelling the effects of potassium metasomatism in sedimentary rocks and paleosols: Implications for paleoweathering conditions and provenance. Geology, 23, 921–924. https://doi.org/10.1130/0091-7613(1995)023<0921:UTEOPM>2.3.CO;2.
[6] Rimmer, S. M. (2004). Geochemical paleoredox indicators in Devonian–Mississippian black shales, Central Appalachian Basin (USA). Chemical Geology, 206, 373–391. https://doi.org/10.1016/j.chemgeo.2003.12.029.
[7] Goldberg, K., & Humayun, M. (2016). Geochemical paleoredox indicators in organic-rich shales of the Irati Formation, Permian of the Paraná Basin, southern Brazil. Brazilian Journal of Geology, 46, 377–393. https://doi.org/10.1590/2317-4889201620160001.
[8] Reyment, R. A. (1965). Aspects of the geology of Nigeria: The stratigraphy of the Cretaceous and Cenozoic deposits. University of Ibadan Press.
[9] Obi, C. G., Okogbue, C. O., & Nwajide, C. S. (2000). Evolution of the Enugu Cuesta: A tectonically driven erosional process. Global Journal of Pure and Applied Sciences, 7, 321–330. https://doi.org/10.4314/gjpas.v7i2.16251.
[10] Murat, R. C. (1972). Stratigraphy and paleogeography of the Cretaceous and Lower Tertiary in southern Nigeria. In T. F. J. Dessauvagie & A. J. Whiteman (Eds.), African geology (pp. 251–266). University of Ibadan Press.
[11] Nwajide, C. S., & Reijers, T. J. (1996). Geology of the southern Anambra Basin. In Selected chapters on geology: Sedimentary geology and sequence stratigraphy in Nigeria and three case studies.
[12] Petters, S. W. (1991). Stratigraphic evolution of the Benue Trough and its implication for Upper Cretaceous palaeogeography of West Africa. Journal of Geology, 86, 311–322. https://doi.org/10.1086/649693.
[13] Dim, C., Okogbue, C. O., Umeji, A., Okeugo, C., & Ogah, J. (2013). Sequence stratigraphy and petroleum potential of Cretaceous strata in the Anambra Basin, southeastern Nigeria. Journal of Geology Research, 61, 1–10.
[14] Akinyemi, S., Adebayo, O., Ojo, O., Fadipe, O., & Gitari, W. (2013). Mineralogy and geochemical appraisal of paleo-redox indicators in Maastrichtian outcrop shales of the Mamu Formation, Anambra Basin, Nigeria. Journal of Natural Sciences Research, 3, 48–64.
[15] Okiotor, M. E., & Ighodaro, E. J. (2020). Geochemical appraisal of the Mamu Shales exposed around Igodor in the Benin Flank of the Anambra Basin, Nigeria. Journal of Applied Sciences and Environmental Management, 24, 489–493. https://doi.org/10.4314/jasem.v24i3.15.

[16] Jayeola, A. O., Oluwajana, O. A., Olatunji, O. A., Udofia, M. U., & Danjuma, O. (2016). Sedimentological, palynological, and foraminiferal biostratigraphic studies of the Upper Cretaceous Mamu Formation at Imiegba, Anambra Basin, Edo State, Nigeria. Achievers Journal of Scientific Research, 1, 37–56.
[17] Akande, S. O., & Mücke, A. (1993). Mineralogy, petrography, and genesis of some Nigerian coals. International Journal of Coal Geology, 23, 93–115.
[18] Dim, C.I.P., Mode, A.W. & Okwara, I.C. Signatures of key petroleum system elements: outcrop examples from the Anambra Basin, Southeastern Nigeria. *J Petrol Explor Prod Technol* 9, 1615–1631 (2019). https://doi.org/10.1007/s13202-018-0589-2.
[19] Edegbai, A., Oboh-Ikuenobe, F. E., & Obi, C. G. (2019a). Palynofacies and paleoenvironmental interpretation of Upper Cretaceous sediments from the Anambra Basin, southeastern Nigeria. Journal of African Earth Sciences, 150, 727–744.
[20] Tijani, M. N., Onodera, S., & Adeleye, M. A. (2010). Hydrochemical and stable isotope assessment of groundwater quality in a basement complex terrain, southwestern Nigeria. Hydrogeology Journal, 18, 453–470.
[21] Mode, A. W., & Odumodu, C. F. R. (2015). Lithofacies and ichnology of the Late Maastrichtian–Danian Nsukka Formation in the Okigwe area, Anambra Basin, southeastern Nigeria. Arabian Journal of Geosciences, 8, 7455–7466. https://doi.org/10.1007/s12517-014-1742-y.
[22] Obaje, N. G. (2009). Geology and mineral resources of Nigeria. Springer. https://doi.org/10.1007/978-3-540-92685-6.
[23] Nwajide, C. S. (2005). Anambra Basin of Nigeria: Synoptic basin analysis as a basis for evaluation of hydrocarbon prospectivity. In C. O. Okogbue (Ed.), Hydrocarbon potentials of the Anambra Basin (pp. 2–46). Great AP Express Publishers.
[24] Loubser, M., & Verryn, S. (2008). An evaluation of some South African Permian coals by organic petrology, geochemistry and FTIR spectroscopy. International Journal of Coal Geology, 75, 1–14.
[25] Hayashi, K.-I., Fujisawa, H., Holland, H. D., & Ohmoto, H. (1997). Geochemistry of ~1.9 Ga sedimentary rocks from northeastern Labrador, Canada. Geochimica et Cosmochimica Acta, 61, 4115–4137. https://doi.org/10.1016/S0016-7037(97)00214-7.
[26] Scotese, C. R., Song, H., Mills, B. J. W., & van der Meer, D. G. (2021). Phanerozoic paleotemperatures: The Earth's changing climate during the last 540 million years. Earth-Science Reviews, 215, 103503. https://doi.org/10.1016/j.earscirev.2021.103503.
[27] Jones, B., & Manning, D. A. C. (1994). Comparison of geochemical indices used for the interpretation of palaeoredox conditions in ancient mudstones. Chemical Geology, 111, 111–129. https://doi.org/10.1016/0009-2541(94)90085-X.
[28] Wignall, P. B., & Maynard, J. R. (1993). The sequence stratigraphy of transgressive black shales. In B. J. Katz & L. M. Pratt (Eds.), Source rocks in a sequence stratigraphic framework (pp. 35–47). AAPG Studies in Geology. https://doi.org/10.1306/St37575C4.
[29] Li, D., Li, R., Zhu, Z., Wu, X., Liu, F., Zhao, B., Cheng, J., & Wang, B. (2018). Elemental characteristics and paleoenvironment reconstruction: A case study of the Triassic lacustrine Zhangjiatan oil shale, southern Ordos Basin, China. Acta Geochimica, 37, 134–150. https://doi.org/10.1007/s11631-017-0193-z.
[30] Dymond, J., Suess, E., & Lyle, M. (1992). Barium in deep-sea sediment: A geochemical proxy for paleoproductivity. Paleoceanography, 7, 163–181. https://doi.org/10.1029/92PA00181.
[31] Obi, C. G. (2000). Depositional model for the Campanian–Maastrichtian Anambra Basin, southeastern Nigeria [Doctoral dissertation, University of Nigeria, Nsukka].